Light curves and radio structure for the September 1999 transient event in XTE J1819-254 (=SAX J1819.3-2325 = V4641 Sagittarii)

Hjellming, R.M.; Rupen, M.P.; Hunstead, R.W.; Campbell-Wilson, D.; Mioduszewski, A.J.; Gaensler, B.M.; Smith, D.A.; Sault, R.J.; Fender, R.P.; Spencer, R.E.; de la Force, C.J.; Richards, A.M.S.; Garrington, S.T.; Trushkin, S.; Ghigo, F.D.; Waltman, E.B.; McCollough, M.

DOI
10.1086/317255

Publication date
2000

Published in
Astrophysical Journal

THE ASTROPHYSICAL JOURNAL, 544:977–992, 2000 December 1

LIGHT CURVES AND RADIO STRUCTURE OF THE 1999 SEPTEMBER TRANSIENT EVENT IN V4641 SAGITTARII (=XTE J1819−254=SAX J1819.3−2525)

R. M. HJELLMING[1] AND M. P. RUPEN
National Radio Astronomy Observatory,[2] Socorro, NM 87801; rhjellmi@nrao.edu, mrupen@nrao.edu

R. W. HUNSTEAD, D. CAMPBELL-WILSON, AND A. J. MIODUSZEWSKI
School of Physics, University of Sydney, Sydney, NSW 2006, Australia; RWH@physics.usyd.edu.au, amiodusz@nrao.edu

B. M. GAENSLER[3] AND D. A. SMITH
Center for Space Research, Massachusetts Institute of Technology, Cambridge, MA 02139; bmg@space.mit.edu, dasmith@space.mit.edu

R. J. SAULT
Australia Telescope National Facility,[4] Epping, NSW 1710, Australia; rsault@csiro.atnf.au

R. P. FENDER
University of Amsterdam, Amsterdam 1098 SJ, Netherlands; rpf@astro.uva.nl

R. E. SPENCER, C. J. DE LA FORCE, A. M. S. RICHARDS, AND S. T. GARRINGTON
University of Manchester, Jodrell Bank Observatory, UK; res@jb.man.ac.uk, cjd@jb.man.ac.uk, amsr@jb.man.ac.uk, stg@jb.man.ac.uk

S. A. TRUSHKIN
Special Astrophysical Observatory, RAS, Nizhnij Arkhyz, Karachaevo-Cherkassia 369167, Russia; satr@cats.sao.ru

F. D. GHIGO
National Radio Astronomy Observatory, Green Bank, WV 24944; fghigo@nrao.edu

E. B. WALTMAN
Remote Sensing Division, Naval Research Laboratory,[5] Washington, DC 20375; ewaltman@rsd.nrl.navy.mil

AND

M. MCCOLLOUGH
Universities Space Research Association, Huntsville, AL 35812; Michael.McCollough@msfc.nasa.gov
Received 2000 May 9; accepted 2000 June 6

ABSTRACT

We report on radio observations of the 1999 September event of the X-ray transient V4641 Sgr (=XTE J1819−254=SAX J1819.3−2525). This event was extremely rapid in its rise and decay across radio, optical, and X-ray wavelengths; the X-rays rose to 12 crab within 8 hr and faded to below 0.1 crab in less than 2 hr. Radio observations were made with seven telescopes during the first day following the onset of the strong X-ray event, revealing a strong radio source that was detected for 3 further weeks by the more sensitive telescopes. The radio source was resolved even in the first Very Large Array (VLA) images (September 16.027 UT), being $\sim 0\farcs25$ long with an axis ratio of at least 10:1. The total flux density decayed by a factor of ~ 4 over the first day, and by September 17.94 UT the radio emission was confined to a slowly decaying, marginally resolved remnant located at one side of the early elongated emission. The H I absorption spectrum gives a minimum kinematic distance of about 400 pc; various other arguments suggest that the true distance is not much greater than this.

The inferred proper motions for the early extended emission ($0\farcs4$–$1\farcs1$ day^{-1}) correspond to $v/c \sim 1.0$–3.2 (d/0.5 kpc), and this together with the radio morphology argues that this is a relativistic jet source like GRS 1915+105 and GRO J1655−40. The proper motion of the late-time remnant is at least 100 times smaller. One simple interpretation posits the ejection of a single short-lived jet segment, followed by a more slowly decaying, optically thin jet segment ejection. These two components can explain both the multifrequency radio light curves and the radio images. The most likely parameters for the fast-jet system with net-averaged proper motion of $\sim 0\farcs4$ day^{-1}, assuming $d = 0.5$ kpc, are $v \sim 0.85c$ and $i \sim 63°$, where i is the inclination to the line of sight. The corresponding apparent velocities are $1.4c$ and $0.6c$ for the approaching and receding jets, making V4641 Sgr the closest superluminal jet source known.

Subject headings: black hole physics — gamma rays: bursts — radio continuum: stars — X-rays: bursts — X-rays: stars

1. INTRODUCTION

A new X-ray transient was independently discovered in 1999 February by *BeppoSax*, designated SAX J1819.3−2525 (in 't Zand et al. 1999), and the *Rossi X-Ray Timing Explorer* (*RXTE*) Proportional Counter Array (PCA), designated XTE J1819−254 (Markwardt, Swank, &

[1] Deceased.
[2] Operated by Associated Universities, Inc., under cooperative agreement with the National Science Foundation.
[3] Hubble Fellow.
[4] The Australia Telescope is funded by the Commonwealth of Australia for operation as a National Facility managed by CSIRO.
[5] Radio astronomy at the Naval Research Laboratory is supported by the Office of Naval Research.

Marshall 1999). Its early X-ray flux density varied between less than 1 and 80 mcrab. On 1999 September 15–16 the *RXTE* All-Sky Monitor (ASM) detected a very strong X-ray event (Smith, Levine, & Morgan 1999; D. A. Smith et al. 2000, in preparation; Wijnands & van der Klis 2000) that reached a flux density of 12 crab and was above 1 crab for only a few hours. In the previous weeks variable star observers, who thought they were observing the variable star GM Sagittarii, had noted enhanced and variable activity in a star studied by Goranskij (1978, 1990)—later designated V4641 Sgr (Green 1999). Williams (1999) remeasured a position for Goranskij's star, $\sim 32''$ from GM Sgr, and pointed out that Goranskij's star was probably the active star. A 0.4 Jy radio counterpart was found by Hjellming, Rupen, & Mioduszewski (1999) and confirmed by Gaensler et al. (1999) at the position of V4641 Sgr (Goranskij 1978; Williams 1999).

On 1999 September 15.395 UT, the star now designated V4641 Sgr was found to have increased rapidly in optical brightness, to 1.1 Jy (Stubbings 1999; Kato et al. 1999); the optical flux density then decayed by a factor of about 4 over the next 12 hr. At the same time as the initial optical flare was detected, the *RXTE* ASM saw the beginning of the 2–12 keV X-ray flux increase from 0.2 to 12.2 crab over a period of 8 hr (Smith et al. 1999; D. A. Smith et al. 2000, in preparation). Less than 2 hr after the peak of the very bright X-ray flare, the X-ray flux seen by the *RXTE* ASM rapidly declined to below 0.1 crab. Further analysis of the *RXTE* ASM data showed an earlier 4.5 crab event at 1999 September 14.89 UT, which lasted less than 3 hr. These events were also detected by *Compton Gamma Ray Observatory* (*CGRO*) Burst and Transient Source Experiment (BATSE; McCollough, Finger, & Woods 1999). The 20–100 keV *CGRO* BATSE and 2–12 keV *RXTE* ASM light curves are plotted as a function of UT time and Modified Julian Day (MJD = JD − 2,400,000.5) in Figure 1*a* and 1*b*, together with spectral hardness (Fig. 1*c*) as determined from the *RXTE* ASM data. The visual light curve (Kato et al. 1999) is plotted in Figure 1*d*. The last panel (Fig. 1*e*) displays some of the radio data and the best-fit model light curves (discussed in detail below).

This paper deals mainly with the very fast radio event in V4641 Sgr. We discuss first the evolution of the radio flux density and the relationships (see Fig. 1) between the radio, X-ray, and optical outbursts. We then turn to the extraordinary Very Large Array (VLA) images of the radio emission, which showed the source to be highly elongated and already quite extended ($0''.25$) within a day of the September 15.3 UT X-ray flare. Within 2 more days this extended source had vanished, leaving behind a stationary, marginally resolved, and more slowly decaying remnant which persisted for at least 26 more days. We show that both the radio morphology and the multifrequency radio light curves can be fitted by a simple two-component model and interpret the emission as the superposition of a relatively short-lived superluminal jet segment and a more slowly decaying jet segment that appears only in optically thin decay. We conclude by discussing the implications for other X-ray transients.

In this paper we refer to the X-ray, radio, and optical transient as V4641 Sgr, even though that name was not assigned (Green 1999) until 6 weeks after the 1999 September 14–16 events. Because of the many references to times, we will also often leave out the year and month when referring to a specific date, so for example, 15.997 UT means 1999 September 15.997 UT.

2. THE RADIO, OPTICAL, AND X-RAY LIGHT CURVES

2.1. *The Radio Data*

The rapid announcement and exchange of information by e-mail about the V4641 Sgr X-ray, optical, and radio event allowed seven radio telescopes around the world to observe the source within 24 hr of the initial X-ray detection. The full set of radio data are plotted in Figure 2, and most are also listed in Table 1.

The first radio detection was by the Green Bank two-element interferometer (GBI) on 15.997 UT when V4641 Sgr was a 0.36 Jy radio source at 8.3 GHz. The GBI also detected it at 2.25 GHz, but flux densities at that frequency are not reported here because of the contamination by the strong radio source J1820−2528 located $22'$ east of V4641 Sgr. By 16.065 UT the source had fallen to 0.27 Jy at 8.3 GHz, and when next observed by the GBI 2 days later, it was 0.012 Jy. After that the source was too weak to determine anything but large upper limits from the GBI data.

The VLA in its 36 km configuration observed V4641 Sgr at 1.42, 4.9, and 14.9 GHz from 16.020 to 16.053 UT. Two epochs at each frequency were separated by 30 minutes; it was steady at 0.34 Jy at 1.42 GHz but decayed from 0.42 to 0.40 Jy at 4.9 GHz between 16.027 UT and 16.048 UT and from 0.24 to 0.20 Jy at 14.9 GHz between 16.032 UT and 16.053 UT. The next telescope to observe the radio source was the Molonglo Observatory Synthesis Telescope (MOST) which, during the period 16.20 ± 0.10 UT, detected a 0.28 Jy source at 843 MHz with no discernible variations. On September 16.16 UT, Djorgovski et al. (1999) used the Owens Valley Radio Observatory (OVRO) 40 m telescope to detect a mean flux density of 0.084 Jy at an average frequency of 30 GHz. At the same time, the Australia Telescope Compact Array (ATCA) began a remarkable series of observations showing that the radio source declined from 0.31 to 0.21 Jy at 1.4 GHz between 16.16 UT and 16.55 UT and from 0.25 to 0.13 Jy at 8.6 GHz between 16.21 UT and 16.40 UT.

The next radio observations of V4641 Sgr were made at 16.66 UT with the RATAN 600 m telescope at 0.96, 2.3, 3.9, 7.7, and 11.2 GHz, measuring flux densities of 0.30, 0.16, 0.095, 0.05, and 0.04 Jy, respectively. One day later the source had fallen to 0.035 Jy at 3.9 GHz. The 16.66 UT data points were interpolated in frequency using the power law $0.3\nu_{\rm GHz}^{-0.85}$ Jy to derive the flux densities at 1.4, 4.9, 8.4, and 14.9 GHz, which are plotted in Figure 2.

The MERLIN array followed next, observing with one antenna pair between 16.729 and 16.896 UT and detecting a decline from 0.14 to 0.11 Jy at 1.42 GHz. The same MERLIN antenna pair also made 1.42 GHz observations between 17.708 and 17.896 UT, yielding a mean flux density of 0.075 Jy.

After September 16 the MOST observed the decay of the radio source at 843 MHz, obtaining flux densities of 0.12, 0.058, and 0.021 Jy on 17.21, 18.16, and 20.20 UT, respectively. The VLA also continued to observe, tracking the decay at 1.42, 4.9, 8.46, and 14.9 GHz. These data, together with those from the other six radio telescopes, are plotted in Figure 2 and listed in Table 1. VLA observations were discontinued after October 7.95 UT, when V4641 Sgr had decayed to 0.13 mJy, because the optically thin decay curve

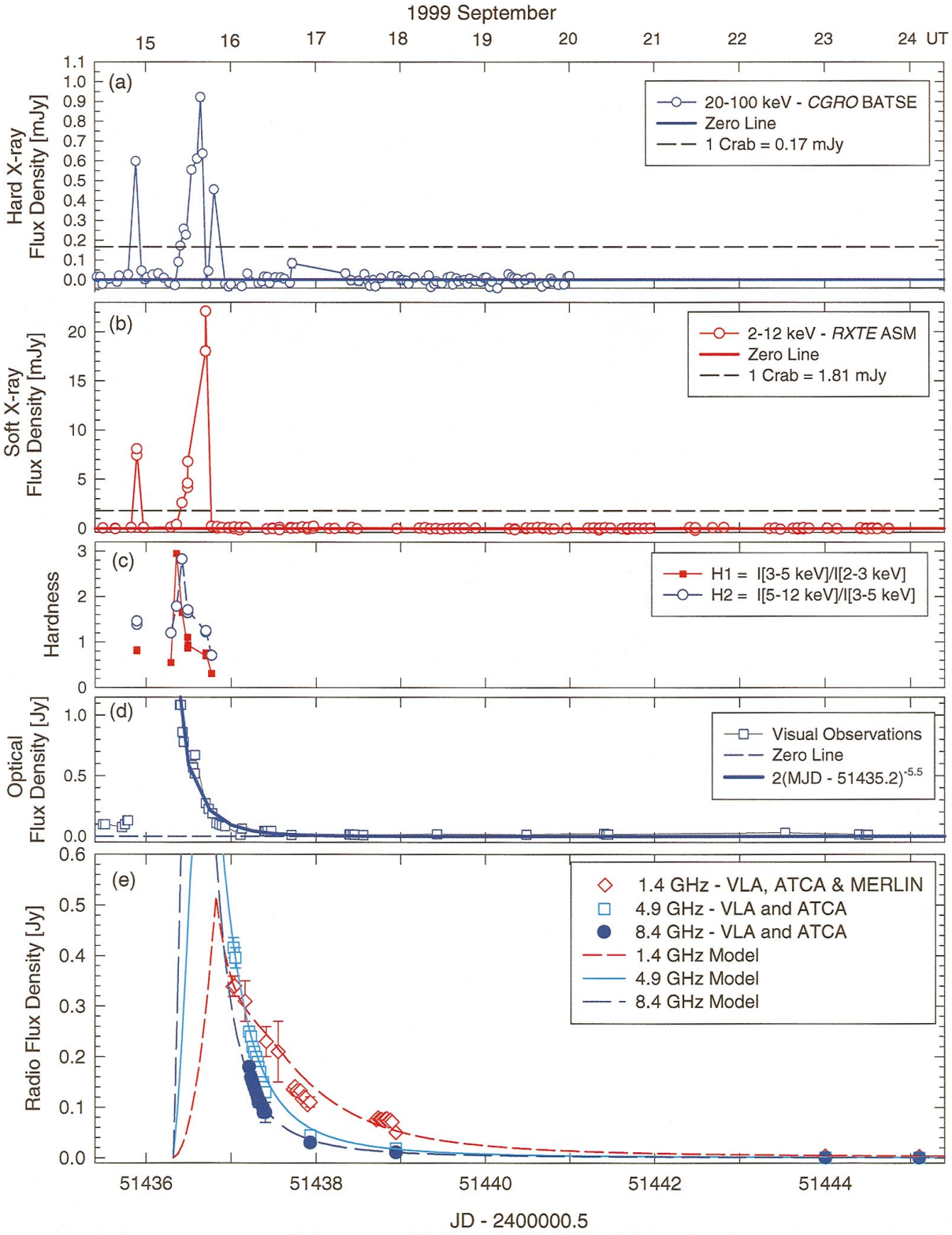

FIG. 1.—V4641 Sgr light curves for (*a*) hard X-ray (*CGRO* BATSE, 20–100 keV); (*b*) soft X-ray (*RXTE* ASM, 2–12 keV); (*c*) *RXTE* ASM hardness (H1 = I[3–5 keV]/I[2–3 keV], H2 = I[5–12 keV]/I[3–5 keV]); (*d*) visual flux density; and (*e*) radio flux density for three of the observed frequencies—all plotted in units of janskys or millijanskys as a function of UT time (*top axis*) and MJD = JD − 2,400,000.5 (*bottom axis*). The lines in (*e*) show the models for the plotted frequencies that fit both the radio light curve data and the observed images' structures (see § 4.3.3).

was reasonably well established, and it was becoming difficult to get long enough observing periods on the VLA. The radio data after 16.4 UT, for all frequencies $\nu \geq 1.4$ GHz, are roughly fitted by the empirical decay formula $\sim 0.24 \nu_{\rm GHz}^{-0.75}({\rm MJD} - 51{,}436.9)^{-1.9}$ Jy, with uncertainties of ± 0.05 for both the spectral index and the power-law decay index.

The lines in the radio light curves in Figure 1*e* are derived from a model consisting of an optically thin remnant and a 0.3 day, $\simeq 0.85c$ ejection of a finite conical jet of relativistic

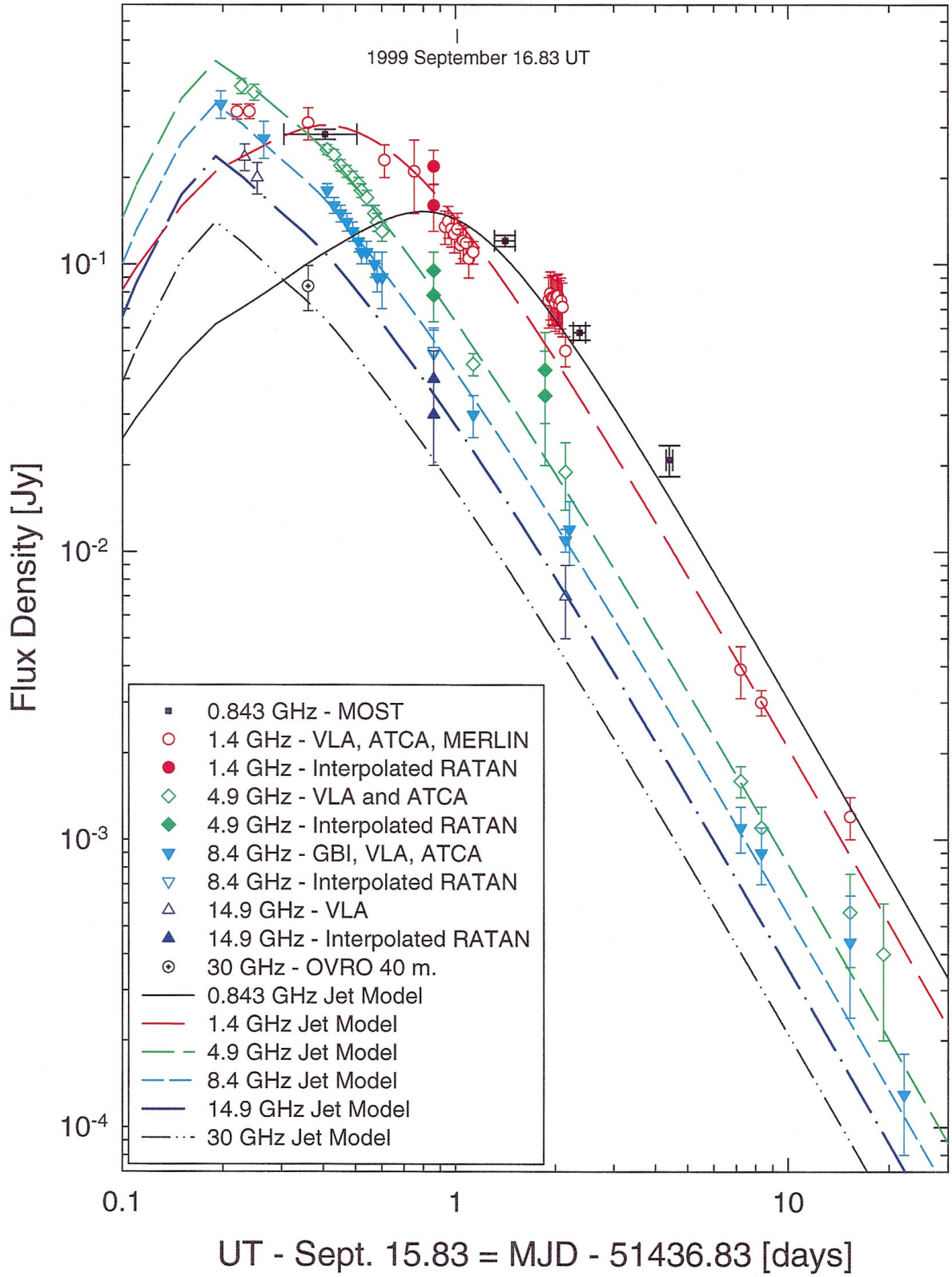

FIG. 2.—The radio flux densities in janskys plotted as a function of MJD − 51,436.83, where the symbols are the measurements from each of the seven radio telescopes and the lines are based on a single-event, finite jet segment model fitted to the data (see § 4.3).

electron plasma, emitting first optically thick, then optically thin synchrotron radio emission. The lines in Figure 2 are based on a single jet ejection model, which fits many but not all of these photometric data and fails to predict some of the main features in the observed images. This model, and the two-component model used in Figure 1*e*, are discussed in § 4.3.

2.1.1. *The* H I *Absorption Spectrum*

The 21 cm H I absorption against V4641 Sgr was

TABLE 1

RADIO OBSERVATIONS OF V4641 SGR

1999/Month/Day (days)	Telescope	ν (GHz)	$S_{0.8}$ (mJy)	$S_{1.4}$ (mJy)	S_5 (mJy)	S_8 (mJy)	S_{15} (mJy)
MJD 51,436:							
09/15.997	GBI	8.3				360 ± 50	
MJD 51,437:							
09/16.020	VLA	1.42		340 ± 20			
09/16.027	VLA	4.9			420 ± 20		
09/16.032	VLA	14.9					240 ± 20
09/16.040	VLA	1.42		340 ± 20			
09/16.048	VLA	4.9			400 ± 20		
09/16.053	VLA	14.9					200 ± 20
09/16.065	GBI	8.3				270 ± 40	
09/16.160	ATCA	1.4		310 ± 40			
09/16.160	ATCA	2.5		310 ± 20			
09/16.204	MOST	0.843	283 ± 12				
09/16.210	ATCA	4.8			205 ± 10		
09/16.210	ATCA	8.6				180 ± 10	
09/16.230	ATCA	4.8			240 ± 10		
09/16.230	ATCA	8.6				160 ± 10	
09/16.250	ATCA	4.8			220 ± 10		
09/16.250	ATCA	8.6				150 ± 10	
09/16.270	ATCA	4.8			210 ± 10		
09/16.270	ATCA	8.6				140 ± 10	
09/16.290	ATCA	4.8			200 ± 10		
09/16.290	ATCA	8.6				130 ± 10	
09/16.310	ATCA	4.8			190 ± 10		
09/16.310	ATCA	8.6				120 ± 10	
09/16.320	ATCA	4.8			180 ± 10		
09/16.320	ATCA	8.6				110 ± 10	
09/16.340	ATCA	4.8			170 ± 10		
09/16.340	ATCA	8.6				110 ± 10	
09/16.370	ATCA	4.8			150 ± 10		
09/16.370	ATCA	8.6				100 ± 10	
09/16.380	ATCA	4.8			140 ± 10		
09/16.380	ATCA	8.6				90 ± 10	
09/16.400	ATCA	4.8			130 ± 10		
09/16.400	ATCA	8.6				90 ± 10	
09/16.410	ATCA	1.4		230 ± 20			
09/16.410	ATCA	2.5		200 ± 10			
09/16.550	ATCA	1.4		210 ± 60			
09/16.729	MERLIN	1.42		135 ± 18			
09/16.750	MERLIN	1.42		141 ± 18			
09/16.771	MERLIN	1.42		133 ± 18			
09/16.792	MERLIN	1.42		128 ± 18			
09/16.813	MERLIN	1.42		133 ± 18			
09/16.833	MERLIN	1.42		117 ± 17			
09/16.854	MERLIN	1.42		121 ± 17			
09/16.875	MERLIN	1.42		119 ± 17			
09/16.896	MERLIN	1.42		105 ± 15			
09/16.930	VLA	1.42		110 ± 10			
09/16.930	VLA	4.9			45 ± 4		
09/16.930	VLA	8.46				30 ± 5	
MJD 51,438:							
09/17.211	MOST	0.843	121 ± 5				
09/17.708	MERLIN	1.42		75 ± 15			
09/17.729	MERLIN	1.42		79 ± 15			
09/17.750	MERLIN	1.42		77 ± 15			
09/17.771	MERLIN	1.42		76 ± 15			
09/17.792	MERLIN	1.42		74 ± 15			
09/17.813	MERLIN	1.42		76 ± 15			
09/17.833	MERLIN	1.42		78 ± 15			
09/17.854	MERLIN	1.42		73 ± 15			
09/17.875	MERLIN	1.42		74 ± 15			
09/17.896	MERLIN	1.42		71 ± 15			
09/17.940	VLA	1.42		50 ± 6			
09/17.940	VLA	4.9			19 ± 5		

TABLE 1—*Continued*

1999/Month/Day (days)	Telescope	ν (GHz)	$S_{0.8}$ (mJy)	$S_{1.4}$ (mJy)	S_5 (mJy)	S_8 (mJy)	S_{15} (mJy)
09/17.940	VLA	8.46				11 ± 1	
09/17.940	VLA	14.9					7 ± 2
MJD 51,439:							
09/18.000	GBI	8.3				12 ± 3	
09/18.164	MOST	0.843	58 ± 3.4				
MJD 51,441:							
09/20.204	MOST	0.843	21 ± 2.6				
MJD 51,444:							
09/23.000	VLA	1.42		3.9 ± 0.8			
09/23.000	VLA	4.9			1.6 ± 0.2		
09/23.000	VLA	8.46				1.1 ± 0.2	
MJD 51,445:							
09/24.100	VLA	1.42		3.0 ± 0.3			
09/24.100	VLA	4.9			1.1 ± 0.2		
09/24.100	VLA	8.46				0.9 ± 0.2	
MJD 51,452							
10/01.100	VLA	1.42		1.2 ± 0.2			
10/01.100	VLA	4.9			0.56 ± 0.2		
10/01.100	VLA	8.46				0.44 ± 0.2	
MJD 51,456							
10/06.040	VLA	4.9			0.4 ± 0.2		
MJD 51,464:							
10/07.950	VLA	8.46				0.13 ± 0.05	

observed with the VLA on 17.9 UT, by which time the source had decayed to 0.037 Jy at 1.4 GHz. The absorption spectra toward V4641 Sgr and the nearby extragalactic radio source J1820−2528 are shown in Figure 3. All the features seen toward the extragalactic source are also present toward V4641 Sgr. The corresponding (minimum) kinematic distance along this line of sight (Galactic coordinates $l = 6.^{\circ}77$, $b = -4.^{\circ}79$) is about 400 pc, using the rotation curve of Fich, Blitz, & Stark (1989) and adopting the IAU conventions of 8.5 kpc for the distance to the Galactic center and 220 km s^{-1} for the local rotation speed. The absorption also gives a lower limit on the H I column density of $6.3 \times 10^{20}/(T_{\rm spin}/35\ {\rm K})$ cm^{-2}, where $T_{\rm spin}$ is the spin temperature of the neutral gas, with 35 K a reasonable guess for the cold neutral medium which dominates the absorption (e.g., Kulkarni & Heiles 1988).

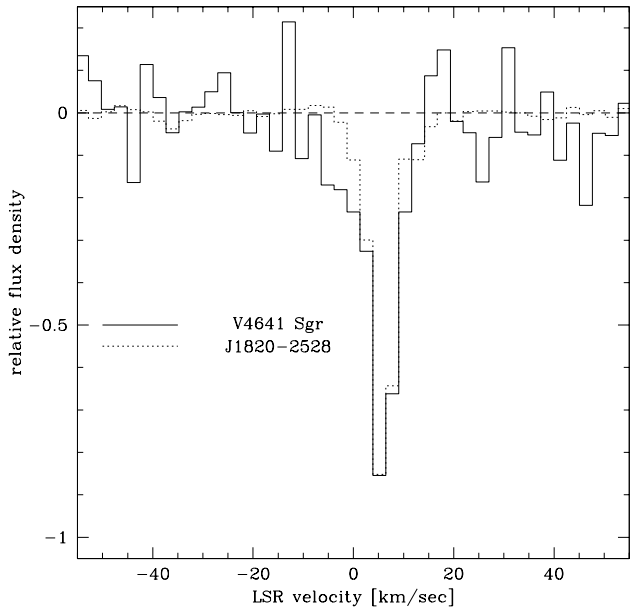

FIG. 3.—H I absorption spectra (flux density vs. LSR velocity) of the radio counterpart of V4641 Sgr (*solid line*) when the radio source was 37 mJy, and the calibrator J1820−2528 (*dashed line*) located 22′ east of V4641 Sgr. The velocity resolution is 2.6 km s^{-1}.

2.2. *The X-Ray Data*

The BATSE experiment on board *CGRO* (Fishman et al. 1989) was used to monitor the hard X-ray emission from V4641 Sgr. The BATSE Large-Area Detectors (LADs) can monitor the whole sky almost continuously in the energy range of 20 keV to 2 MeV with a typical daily 3 σ sensitivity of better than 100 mcrab. Detector counting rates with a timing resolution of 2.048 s are used for our data analysis. To produce the V4641 Sgr light curve, single step occultation data were taken using a standard Earth occultation analysis technique used for monitoring hard X-ray sources (Harmon et al. 1992). Interference from known bright sources was removed. A spectral analysis of the BATSE data indicated that the data were well fitted by a power law with a photon index of −3.5. The single occultation step data were then fitted with a power law with this index to determine flux measurements in the 20–100 keV band.

The soft X-rays, from 2 to 12 keV, were observed by the ASM experiment on *RXTE* and are plotted in Figure 1*b*. These same data were also used to derive two hardness ratios, based on the ratios of two pairs of flux densities: 3–5/2–3 keV and 5–12/3–5 keV, which are plotted in Figure 1*c*. The BATSE data are plotted in Figure 1*a*.

2.3. *Relationships between the Light Curves*

Figure 1 compares the radio, X-ray, and visual (Kato

et al. 1999) light curves. The optical light curve shows an initial level of enhanced optical brightness before the X-ray activity, followed by a sudden brightening to 8.8 mag [=1.1 Jy, using m_V conversion to janskys from Fukugita et. al. 1995, $S(\mathrm{Jy}) = 3590 \times 10^{-m_V/2.5}$] and then a decay within 1 day with an apparent power law of $\sim 2(\mathrm{MJD} - 51{,}435.2)^{-5.5}$ Jy. It is striking that the optical luminosity was already in rapid decline by the time the strongest X-ray event began. This may be because the optical brightening was associated with the weaker X-ray event at September 14.89 UT, but it is also possible that the optical flare, seen only in decay, was a precursor to the largest X-ray outburst. The only other optical observations related to strong X-ray events were those of the 1996 X-ray outburst in GRO J1655−40 (Orosz et al. 1997; Esin et al. 2000) and the 2000 outburst in XTE J1550−564 (Jain & Bailyn 2000). In the case of GRO J1655−40, there was an exponential rise in optical luminosity that began 6 days before the X-ray outburst detected by the *RXTE* ASM and a very long ∼100 day optical decay following the reappearence of the soft X-ray source. In the case of XTE J1550−564, the optical counterpart was seen to have brightening before and decay after the X-ray outburst. Except for previously studied sources like V4641 Sgr, where variable star observers regularly monitor optical activity and unusual but well-known sources like GRO J1655-40 and XTE J1550−564, X-ray transients are seldom observed just before their X-ray outbursts. The rapid optical decay seen here, preceding the strong X-ray outburst, could be a general feature of such outbursts.

A better established correlation in other X-ray transients is that between the initial production of a radio source, usually in the form of the beginning of ejection of a radio-emitting jet, and either the initial appearance of the X-ray source or a sudden quenching of hard X-rays (Harmon et al. 1995; Hjellming & Rupen 1995; Hjellming 1996; Kuulkers et al. 1999). In V4641 Sgr (Fig. 1), an initial very brief 4.5 crab event on 14.89 UT was seen by both ASM and BATSE, but the strongest X-ray emission appeared in both soft and hard X-rays at 15.3 UT, followed by a sudden drop from peak flux levels between 15.70 and 15.77 UT. This decline also seems to have been simultaneous at 20–100 keV and 2–12 keV, but another very transient rise at 20–100 keV occurred on 15.8 UT, during a gap when V4641 Sgr was outside the *RXTE* ASM field of view.

Since no telescope caught the beginning of the radio event, it is difficult to make a direct connection between this and one of these well-defined X-ray features. However, the rapid radio decay, the radio images discussed in the next section, and what is known about other X-ray/radio correlations all suggest that most of the jet ejection seen in the radio light curves began either about the time of the strong X-ray rise starting at 15.3 UT or during the strong X-ray quenching near 15.8 UT. The detailed model fitting discussed in § 4.3 gives an independent estimate that the main jet ejection event began about 15.32 UT (Fig. 1*e*); this seems quite plausible and implies that the most likely association is with the strong X-ray rise, as the hardness plotted in Figure 1*c* peaked and was beginning to decay.

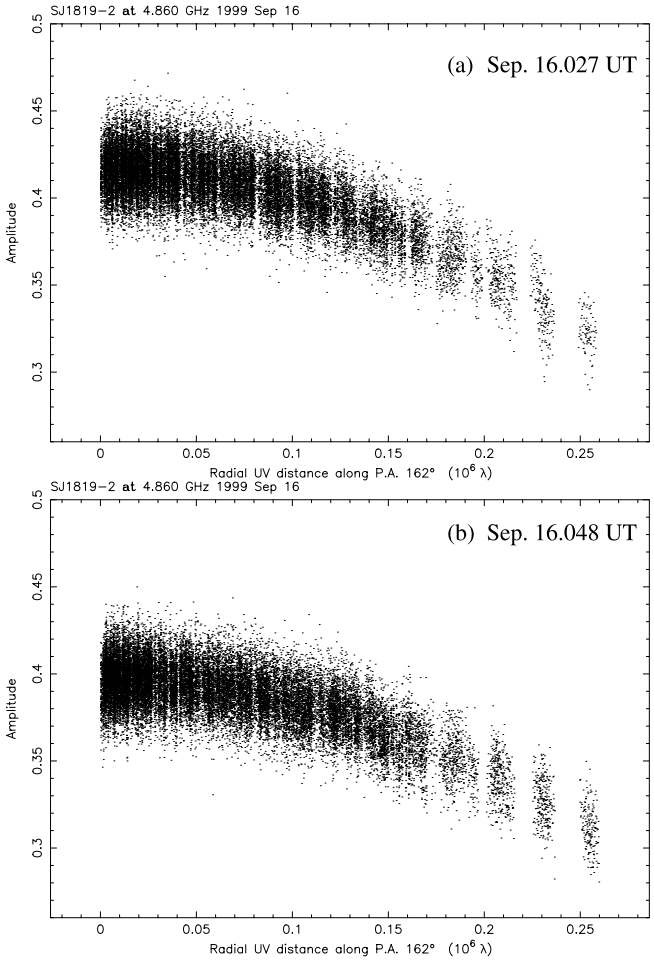

FIG. 4.—Plots of the 4.9 GHz amplitudes as a function of baseline length projected along an axis at a position angle of 162° for (*a*) 1999 September 16.027 UT and (*b*) 1999 September 16.048 UT. The decline of the observed amplitude for longer baselines is an unambiguous sign that the source is resolved; a point source would appear as a horizontal line (apart from thermal noise).

3. THE STRUCTURE OF THE RAPIDLY CHANGING RADIO SOURCE

3.1. *September 16.027 and 16.048: A Resolved, Highly Elongated Jet*

3.1.1. *The Visibility Data*

The first VLA observations of V4641 Sgr were made on 16.027 and 16.048 UT, less than a day after the beginning of the X-ray outburst which triggered those observations. Astonishingly, the source was already resolved. This can be seen directly from the calibrated 4.9 GHz visibility data. Note that calibration for V4641 Sgr is straightforward and reliable, since the source is only 22′ away from the strong (∼1 Jy) pointlike calibrator J1820−2528, whose position is determined from VLBI measurements to better than 2 mas. This calibrator was observed immediately before each of the scans discussed here.

Figure 4 shows plots of the 4.9 GHz visibility amplitude as a function of the absolute value of the projected distance between antenna pairs, in units of the observing wavelength, for two 7 minute scans taken on 16.027 (*top*) and 16.048 (*bottom*) UT. Each point represents a 10 s integration. The ordinate is the projection of the baseline length along a position angle (P.A.) of 162°. A point source, such as a calibrator, would appear as a horizontal line (i.e., have the

same amplitude for all projected distances), with some scatter due to the thermal noise. The fact that the observed visibilities fall off as the projected baseline length increases is the clear and unambiguous sign of a resolved source. Figure 4*a* indicates that on September 16.027 the total flux density of the radio source was 0.42 Jy at 4.9 GHz, while the amplitudes for long north-south baselines fall to about 0.3 Jy; 30 minutes later (Figure 4*b*), the total flux density had declined to 0.40 Jy and the amplitude on the longest north-south baselines had fallen to 0.28 Jy.

The qualitative behavior seen in Figure 4 could be produced by any number of source structures—an elliptical Gaussian, a double or a triple radio source—all oriented at a position angle near 162° and with size or separations of $\sim 0\farcs25$. To be more quantitative, the AIPS program OMFIT was used to perform least-squares fits of these simple models to the visibility data. The results for a single elliptical Gaussian model are shown in the second and third columns of Table 2. Fits using two point sources gave much larger values for the reduced χ^2; using three point sources was better but gave large errors for one component. After some trial and error, it was found that the best fits (signficantly better than for a single Gaussian) were obtained by using two point sources and an elliptical Gaussian, with the two point sources held at the same positions in each scan; the results are given in the fourth and fifth columns of Table 2. In these models, one point source was held fixed at the radio centroid, $\alpha = 18^{\rm h}19^{\rm m}21\fs634$, $\delta = -25°24'25\farcs60$ (J2000), and the other at the position of radio emission seen on and after September 17.94 UT (see below), $\alpha = 18^{\rm h}19^{\rm m}21\fs642$, $\delta = -25°24'25\farcs85$ (J2000).

These three-component fits indicate that two things changed in a period of 30 minutes: the centroid of the elongated Gaussian moved along the direction of the major axis, which is on average 166° from the model fits and 162° from the visibility plots; and the flux density of the Gaussian decreased by 28 mJy, reflecting most of the change in the total flux over that same time period. The major axis of the Gaussian is $\sim 0\farcs47$ and does not significantly change, and the axial ratios are too small to be determinable. These results are qualitatively consistent with the ejection of a highly relativistic jet.

3.1.2. *Images*

Looking at the visibility data directly showed that the radio source was extended and gave some quantitative estimates of its size and structure. But, those estimates depend somewhat on the model which is assumed for the source. In this section, we concentrate instead on making images from the same data, which involves certain technical difficulties but eliminates some of the bias inherent in model fitting.

VLA images made from the September 16.027 and 16.048 UT data at 4.9 GHz using the CLEAN deconvolution algorithm show a strong central radio source and extensions $0\farcs25$ north and south of that source along a position angle of 162°. Unfortunately, the synthesized instrumental beam (point-spread function) itself has an FWHM of $0\farcs8 \times 0\farcs3$ and is elongated at roughly the same position angle (167°). In these circumstances, CLEAN is not reliable, and the structure in these images may easily be a CLEAN artifact.

A much more reliable approach for strong but only marginally resolved sources is the Non-Negative Least Squares (NNLS) algorithm analyzed in detail by Briggs (1995) and implemented in AIPS++. NNLS avoids the instabilities inherent in CLEAN by effectively fitting for all the pixels in the model image simultaneously, rather than iterating one pixel at a time. As discussed in detail by Briggs (1995), this is a much more robust and reliable algorithm for slightly resolved sources, and the resulting images (Figures 5*a* and 5*b*) represent the best estimates available of the underlying source structure. These show an extended jetlike structure with the expected size of about $0\farcs25$ and further suggest that the main morphological distinction between the two epochs was the spreading of the flux in the initial central peak (at 16.027 UT) out along the extended jet.

The first epoch of MERLIN observations on 16.8 UT showed the source varying from 0.14 to 0.11 Jy at 1.42 GHz. With a resolution corresponding to $0\farcs4$, these data are consistent with the size scale and north-south orientation seen in the VLA data earlier the same day. With only a single baseline available, it was not useful to analyze the MERLIN data in any more detail. Similarly, the 14.9 GHz VLA data taken on the same day are significantly less reliable than those at 4.9 GHz, since we had not yet realized the importance of rapid switching at this frequency (see below).

TABLE 2

MODEL FITS FOR 1999 SEPTEMBER 16 UT VLA DATA AT 4.9 GHz

	1 GAUSSIAN		1 GAUSSIAN/2 POINTS	
PARAMETER	16.027 UT	16.048 UT	16.027 UT	16.048 UT
Flux density (Jy)	0.416 ± 0.004	0.350 ± 0.004	0.051 ± 0.0007	0.023 ± 0.0007
$\alpha^{\rm s}$	21.634 ± 0.003	21.636 ± 0.003	21.634 ± 0.003	21.636 ± 0.003
δ''	25.585 ± 0.3	25.595 ± 0.3	25.514 ± 0.002	25.350 ± 0.002
Major axis (arcsec)	0.216 ± 0.02	0.253 ± 0.02	0.49 ± 0.05	0.45 ± 0.05
Axial ratio	0.07 ± 0.08	0.13 ± 0.08	0.0 ± 0.1	0.0 ± 0.1
Major axis P.A. (deg).....	163 ± 0.2	173 ± 0.8	175 ± 0.3	158 ± 1.2
Point Source 1:				
Flux density (Jy)			0.351 ± 0.005	0.354 ± 0.0006
at $\alpha^{\rm s}$.....			21.634	21.634
and δ''			25.60	25.60
Point Source 2:				
Flux density (Jy)			0.018 ± 0.005	0.022 ± 0.0003
at $\alpha^{\rm s}$.....			21.642	21.642
and δ''			25.85	25.85

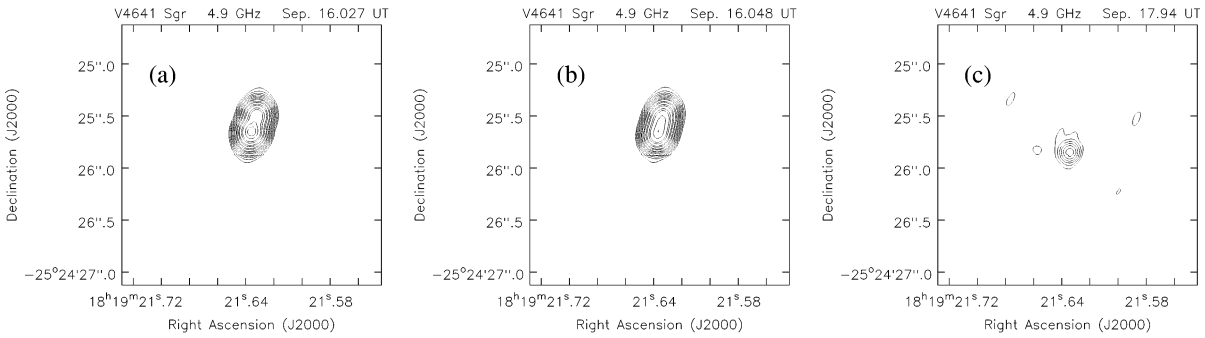

FIG. 5.—(*a*) September 16.027 UT image of V4641 Sgr at 4.9 GHz with peak at 0.248 Jy, contouring at $\pm 2^{n/2} \times 0.005$ Jy for $n = -1, 1, 2, \ldots$; (*b*) September 16.048 UT image at 4.9 GHz with peak at 0.202 Jy, contouring at $\pm 2^{n/2} \times 0.006$ Jy for $n = -1, 1, 2, 3, \ldots$; and (*c*) September 17.94 UT image at 14.9 GHz with peak at 6.7 mJy, contouring at $\pm 2^{n/2} \times 0.0045$ Jy for $n = -1, 1, 2, 3, \ldots$. The restoring beam is a circular Gaussian with a 0".3 FWHM.

The data are, however, consistent with those taken at 4.9 GHz and in themselves clearly suggest a resolved source.

The 16.027 and 16.048 UT images are linearly polarized as shown in Figure 6, where we display the linearly polarized contours and E-field polarization vectors. While the peaks in Figures 6*a* and 6*b* are both 2 mJy, the total linearly polarized flux for the two epochs is 3.7 and 3.1 mJy, respectively, corresponding to the $\sim 1.5\%$ linear polarization and indicating that the polarized emission is slightly resolved. These show that the magnetic fields in the polarized regions have a position angle of about 5°, which is 23° from the position angle of the images in Figure 5. This indicates that the magnetic fields, averaged over the synthesized beam, are elongated roughly but not exactly along the direction of jet motion.

3.2. *September 17.94 UT and Beyond: A Marginally Resolved, Stationary Core*

The next VLA observation took place on 16.94 UT. Unfortunately, by then the radio source had declined to much weaker levels, and the atmosphere above the VLA was exceptionally wet and turbulent because of a passing late-summer storm, so the structure could no longer be seen in the visibility amplitudes; and since the phase self-calibration necessary to remove atmospheric phase variations imposes the structure of any assumed model, required when there is no good initial image, reliable imaging was not possible. Figure 5*c* shows the next image, from 14.9 GHz observations taken on 17.94 UT: the extended component has vanished, leaving only a 7 mJy core located at the southern tip of the September 16 jet. These and subsequent data were taken in a "fast switching" mode, observing the nearby (22′ east) calibrator J1820−2528 every 60 s to ensure accurate phase calibration. Fast switching also ensures good positional accuracy, and the position of the 17.94 UT emission shown in Figure 5*c* is the same as that of all radio emission seen with the VLA between then and October 7.95 UT. The implications of this positional stability are discussed further below.

The mean position of the strongest components in the September 16 1.42, 4.9, and 14.9 GHz VLA data is ($\alpha = 18^h19^m21^s.637$, $\delta = -25°24'25''.60$) (J2000), as reported by Hjellming et al. (1999), with 90% confidence uncertainties of $0^s.007$ and 0".1. We define α^s and δ'' as the seconds and arcseconds parts of J2000 right ascension and declination, so for the above mean position, $\alpha^s = 21^s.637$ and $\delta'' = 25''.60$. Using this notation, the position of the September 17.94 UT core is $\alpha^s = 21^s.634$ and $\delta'' = 25''.85$.

Figure 5*c* and all later images (not shown) were made using the CLEAN algorithm, as the source had become too faint to use NNLS. However, we can still glean some information about the source structure, by noting that the peak

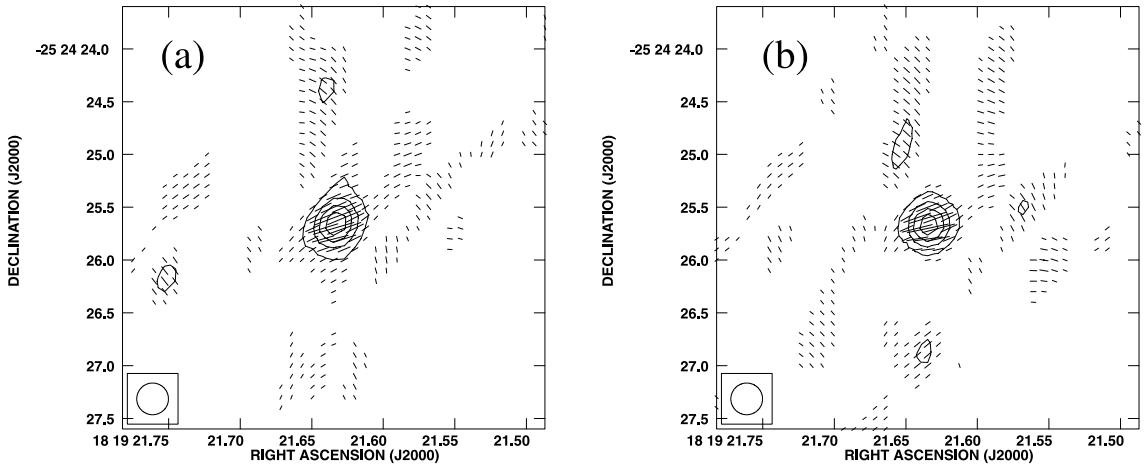

FIG. 6.—Polarization images at 4.9 GHz for (*a*) 16.027 UT and (*b*) 16.048 UT plotted in the form of E-field vectors and polarized intensity contours, where the peaks are 2.0 mJy, the total fluxes are 3.7 and 3.1 mJy, respectively, and the contours are linear multiples of 0.4 mJy.

flux density in the image increases as the image is convolved to lower resolutions. While difficult to quantify, this shows that the late-time radio source is at least marginally resolved, although not nearly as extended as that seen on September 16.

3.3. *Summary of Imaging Results*

The imaging results show that the initial structure contained a one-sided, probably highly relativistic jet, which decayed so rapidly as to be unobservable 1.9 days later. Subsequent images show a marginally resolved, stationary remnant left behind at the southern tip of the original jet, presumably associated with the core. The interpretation of these images, in the context of the radio light curves, is the subject of the next section.

4. THE NATURE OF THE RADIO SOURCE

The most striking features of the radio source associated with V4641 Sgr are

1. High surface brightness and linear polarization indicating synchrotron emission from a highly relativistic electron plasma with magnetic fields;
2. The presence of extended, highly elongated emission less than a day after the earliest likely ejection date, and only a half day after the most probable ejection data;
3. The rapid disappearance of the early extended emission within the following two days; and
4. The continued presence and gradual decay of a marginally resolved, stationary component for at least an additional 26 days thereafter. This component is located near the southern tip of the original, much more extended emission.

The rapid appearance of extended, roughly linear structure strongly suggests a relativistic jet like those associated with other X-ray transients. Both its apparent speed and the presumed association between the long-lived remnant and the original ejection site argue for the importance of relativistic effects such as beaming and time dilation, while adiabatic losses could easily explain its rapid decay. The longer lived remnant, on the other hand, must move rapidly enough to decay and become slightly resolved, while appearing to remain stationary as a whole. A single-ejection model cannot produce this combination because the remnant is more likely to arise from slower ejection of material. It therefore seems as if there are two completely independent sources which happen to coexist; but, if the ongoing ejection is also through a jet, the two may actually be very closely related. SS 433 is an example of a long-lived jet whose ejecta last long enough to be seen a few arcseconds from the core. The superluminal jet sources GRS 1915+105 and GRO J1655−40 both behave similarly, with relatively stable central cores coexisting with the more famous extended jets. In both cases, only the most long-lived ejecta are resolved by the VLA, while VLBI observations show similar jetlike structures which decay too quickly to get out that far.

The remainder of this section is devoted to making these statements more rigorous and complete, first by quantifying the observational constraints and then by formulating a simple model which can explain both the qualitative features of the source and the details of both the radio images and the multifrequency radio light curves. The model is basically that of Hjellming & Johnston (1988), extended to allow for the ejection of finite jet segments (rather than a simple continuous jet) and to account for relativistic effects, including beaming, time dilation, and relativistic radiative transfer along the line of sight.

4.1. *The Distance to V4641 Sgr*

The conversion of angular measurements to linear scales requires knowing the distance to the source. Unfortunately, for V4641 Sgr this distance is only partly constrained. The most direct indicator is the presence of an H I absorption feature at ~ 5 km s^{-1}, which gives a firm lower limit of ~ 0.4 kpc (§ 2.1.1). Various arguments suggest that the true distance cannot be much more than this. First, the Galactic latitude ($-4.^\circ 79$) corresponds to $z = 84(d/1\ \mathrm{kpc})$ pc below the plane at a distance d. Most X-ray transient sources are associated with a disk population with a fairly low scale height; taking $z \lesssim 400$ pc as a reasonable upper limit gives $d \lesssim 5$ kpc. Second, J. Greiner (1999, private communication) has estimated a distance between 0.4 and 1.4 kpc based on the optical spectrum, with the nearer distance being most probable. Third, the angular size of the source, so soon after the X-ray flare, argues for a combination of a close distance and relativistic motion. As discussed in the next subsection, the radio images probably require proper motions of at least $0.''36$ day^{-1}. An apparent speed of $\beta_{\mathrm{app}}c$ therefore requires $d \lesssim 0.5\beta_{\mathrm{app}}$ kpc. Extremely relativistic motions oriented almost directly along the line of sight can give $\beta_{\mathrm{app}} \gg 1$, but this is not very likely for V4641 Sgr, which was selected by its X-ray/optical variability rather than its radio flux. Taking $\beta = 0.995$ and $i = 1^\circ$ would give $\beta_{\mathrm{app}} = 3.4$; even with these extreme values, $d \lesssim 1.7$ kpc. For comparison, the three Galactic sources already known to have highly relativistic, superluminal jets (GRS 1915+105, GRO J1655−40, and XTE J1748−288) would have proper motions of $0.''52$, $0.''41$, and $0.''46$ day^{-1} at a distance of 0.5 kpc (Fender et al. 1999b; Hjellming & Rupen 1995; R. M. Hjellming et al. 2000, in preparation).

In sum, it seems very likely that V4641 Sgr is not too far beyond the minimum distance inferred from the H I absorption spectrum. For the remainder of the paper, we adopt $d = 0.5$ kpc unless otherwise noted.

4.2. *Proper Motion Estimates*

By 16.027 UT, the source was already $\sim 0.''25$ across. What is known about X-ray/radio correlations in other sources suggests that the radio jet ejection began either near the strong X-ray rise starting at 15.3 UT or during the strong X-ray quenching near 15.8 UT (Fig. 1); an association with the very brief 4.5 crab X-ray event on 14.89 UT is possible but less likely. The corresponding proper motion is about

1. $0.''22$ day^{-1} [$\beta_{\mathrm{app}} \sim 0.64(d/0.5\ \mathrm{kpc})$], for ejection on 14.89 UT;
2. $0.''36$ day^{-1} [$\beta_{\mathrm{app}} \sim 1.04(d/0.5\ \mathrm{kpc})$], for ejection on 15.3 UT; or
3. $1.''1$ day^{-1} [$\beta_{\mathrm{app}} \sim 3.2(d/0.5\ \mathrm{kpc})$], for ejection on 15.8 UT.

These are probably underestimates of the true proper motion, since the outer edge of the source may already have decayed below visibility by the time of the first image. The second value of $\sim 0.''36$ day^{-1}, which we round off to $0.''4$ day^{-1}, is the most probable because 15.3 UT will later be

shown to be the most likely time for the beginning of this jet ejection event.

By contrast, the slowly decaying residual source (the remnant) remains at the same position from 17.94 UT through October 7.95 UT, i.e., for a period of 26.0 days. As we will discuss later, this is probably due to a combination of the power-law decay of jet intensity as a function of distance from the point of ejection and the low dynamic range of the very weak source images.

4.3. *A Jet Model Fit to the Radio Light Curves and Images*

Any detailed model for the V4641 Sgr radio source must fit both the overall radio spectral index and decay, embodied in the radio light curves, and the changing radio morphology, as seen in the VLA images. This combination provides strong constraints on possible models, as will be seen below. The most natural model is that of a relativistic, two-sided jet, as seen in SS 433 as well as in numerous X-ray transients and as suggested directly in this source by its elongated, asymmetric structure very soon after the X-ray outburst.

The apparent optically thin decay of $\sim 0.24 \nu_{\rm GHz}^{-0.75}({\rm MJD} - 51{,}436.9)^{-1.9}$ Jy is typical for finite jet segment models (R. M. Hjellming 2000, in preparation). Such a decay can also be produced by a three-dimensional "synchrotron bubble," slowed expansion event with time dependence $\sim (t - t_0)^{-4\gamma/5}$ (Shklovskij 1960; van der Laan 1966; Kellermann 1966; Hjellming & Johnston 1988), where γ is fixed by the observed spectral index α ($S_\nu \propto \nu^\alpha$) to be $-2\alpha + 1 = 2.5$. Apart from not matching the first radio images, however, the synchrotron bubble model predicts ratios for the flux peaks at different frequencies, during the transition from optically thick to optically thin, that are much larger than observed. We will therefore discuss only the finite jet segment model in modeling the jet emission and features in the radio light curves.

4.3.1. *Finite Jet Segment Model for Radio Light Curve Events*

Hjellming & Johnston (1988) developed a model for continuous jet ejection for radio sources such as SS 433. This model predicts extended radio emission with varying rates of power-law decay in the structure of the ejected material. If the supply of relativistic electrons at the base of these jets decreases, these models can match the slow decay of a marginally resolved radio source seen in the V4641 Sgr remnant on and after 17.94 UT. In addition, R. M. Hjellming (2000, in preparation) has recently shown that transient radio events can often be fitted by a simple variant of this model, allowing for the ejection of a finite jet segment which then expands and decays. This provides a natural way to explain the initial jets imaged by the VLA on September 16.

This section summarizes the basic equations for the finite jet segment model, which are applied to V4641 Sgr below. The derivation follows that of Hjellming & Johnston (1988), simply replacing the integral for the flux density with the same integral over changing inner and outer boundaries along the jet axis. One can also apply the Doppler boosting factors appropriate to each part of the jet segment and predict the apparent behavior of relativistic jet events. See R. M. Hjellming (2000, in preparation) for a more complete derivation and discussion.

In order to properly add relativistic effects to the equations of Hjellming & Johnston (1988), one needs to allow for the Doppler factor $\mathscr{D}$ that relates the frequency ν' in the reference frame of the emitting regions to the frequency ν seen by a distant observer. For approaching (+) and receding (−) components, moving with a velocity $v = \beta c$ at an angle θ with respect to the observer's line of sight, the Doppler factor is

$$\mathscr{D}_\pm(t) = \frac{\nu(t)}{\nu'} = \frac{1}{\gamma_L\{1 \pm \beta \cos\,[\theta(t)]\}}\,, \tag{1}$$

where $\gamma_L = (1 - \beta^2)^{-1/2}$ is the Lorentz factor. Precession, or other effects that change the orientation of the jet axis, can make θ, v, and thus $\mathscr{D}$ vary as a function of time t.

In addition, we include a number of features that are reasonable possibilities for transient jet ejection events. The first and most important addition is allowing the jet ejection to begin and end at the times $t_{\rm start}$ and $t_{\rm stop}$. If z is the coordinate along the central axis of the conical jet, let z_1 and z_2 be the inside and outside boundaries of the jet at t. We then express the time dependence of jet ejection by

$$z_2(t) = v(t - t_{\rm start}) + z_0,\ t \geq t_{\rm start}\,, \tag{2}$$

and

$$z_1(t) = v(t - t_{\rm stop}) + z_0 \text{ for } t \geq t_{\rm stop}\,,$$
$$z_1(t) = z_0 \text{ for } t_{\rm start} \leq t \leq t_{\rm stop}\,, \tag{3}$$

where z_0 is an initial value for the location on the jet axis where relativistic plasma is injected. Following the notation of Hjellming & Johnston (1988), r is the radius of the circular cross section of the jet at z, and the adiabatic scalings of relativistic electron energy E, magnetic field H, and the density parameter for relativistic electrons K vary with time according to

$$E(t) = E_0[r(t)/r_0]^{-2/3}\,,$$
$$H(t) = H_0[r(t)/r_0]^{-1}\,,$$
$$K(t) = K_0[r(t)/r_0]^{-2(\gamma+2)/3} f_{\rm injection}(t)\,, \tag{4}$$

where $f_{\rm injection}(t) = 1$ for "sudden" particle injection, and $f_{\rm injection}(t) = t/t_0$ for $t \leq t_{\rm stop}$ and $f_{\rm injection}(t) = t_{\rm stop}/t_0$ for $t > t_{\rm stop}$ for the case of "continuous" injection between $t_{\rm start}$ and $t_{\rm stop}$. Note that $t_0 = z_0/v$, and it is convenient to define the dimensionless axis coordinate $\zeta = z/z_0 = t/t_0$. The expansion of the lateral cross section of the jet can be decelerated by interaction with external gas, so in general $r = r_0(z/z_0)^p = r_0\,\zeta^p$, where $p = 1$, 1/2, or 1/3 for the ideal cases of free lateral expansion, energy conserving lateral expansion, and lateral expansion with conservation of momentum, respectively. The Mach number for the jet is $M_0 = z_0/r_0$, and the angular size scale is $\Theta_0 = z_0/d$, where d is the distance to the source. With these modifications to the equations in Hjellming & Johnston (1988), the flux density from the approaching (+) and receding (−) jets is

$$S_{\nu,\pm}(t) = S_0\, M_0 \left(\frac{\nu}{\nu_0}\right)^{5/2} \sin\,[\theta(t)] \int_{\zeta_1(t)}^{\zeta_2(t)} \mathscr{D}_\pm^{1/2}(t)\zeta^{3p/2} \times \{1 - \exp\,[-\tau'_\nu(t,\,\zeta)]\}\xi_2[\tau'_\nu(t,\,\zeta)]d\zeta\,, \tag{5}$$

where

$$\tau'_{\nu,\pm}(t,\,\zeta) = \left\{\frac{\tau_0\, f_{\rm injection}(t)}{\sin\,[\theta(t)]}\right\}\left(\frac{\nu}{\nu_0}\right)^{\alpha - 5/2} \times \mathscr{D}_\pm^{3/2-\alpha}(t)\zeta^{-(7\gamma+8)p/6}\,, \tag{6}$$

and

$$\xi_2(\tau;\ \tau < 20) \simeq 0.78517 + 0.06273\tau - 0.007242\tau^2 + 0.0003905\tau^3 - 0.00000973\tau^4 + 0.00000009\tau^5 \quad (7)$$

expresses the optical depth dependent correction for the circular cross section of the jet, using the simple formula for a relativistic plasma filling the conical segment of the jet. For $\tau > 20$, $\xi_2(\tau) = 1$. The flux density and optical depth scaling factors S_0 and τ_0 are related to physical parameters by $\tau_0 = 0.038 g(\gamma)(3.5 \times 10^9)^{\gamma} K_0 H_0^{(\gamma+2)/2} r_0$ and $S_0 \cong 1.08 \nu_{0,\mathrm{GHz}}^{5/2} H_{0,\mathrm{mG}}^{-1/2} \gamma^{-3/2} \Theta_{0,\mathrm{mas}}^2$ Jy. The function $g(\gamma) \simeq 0.96\gamma^{-0.5} + 0.0032\gamma^3$ for $1 \leq \gamma \leq 5$. In the above equations, ν_0 is a reference frequency, all of the dependencies on Doppler factors have been included, and the injection of relativistic particles at the base of the jet can be either "sudden," at the beginning of the event, or continuous during the event.

It is important to note that in the optically thin limit of equations (5) and (6), the intensity along each jet segment is proportional to $\zeta^{-(7\gamma-1)p/6}$ (see eqs. [8] and [9] in § 4.3.3), which means that the outermost portions of such a jet segment will be much weaker than the innermost portions, and, in the case of images with limited dynamic range, the outermost portions can be unobservable with respect to the noise.

If $\theta = i$, the angle of the jet axis to the observer's line of sight, there are nine parameters in this finite jet segment model for transient radio events; however, if θ varies with time, there will be additional parameters describing variations with respect to i (Hjellming & Johnston 1988).

In these models the intrinsic emission would be symmetric for approaching and receding jets in their own reference frame. However, two effects make them asymmetric to a distant observer. The effect of the Doppler factor in the radiative transfer equations boosts the strength of the approaching jet relative to the receding jet, and the differential travel time to the observer makes the observer see a "younger" receding jet and an "older" approaching jet. The degree of asymmetry depends only on $\beta \cos[\theta(t)]$, or $\beta \cos i$ for the models without precession or other motions about a mean axis. The Doppler boosting and age factors are clearly seen in the ejections from superluminal sources like GRS 1915+105 and GRO J1655−40 (Mirabel & Rodríguez 1994; Fender et al. 1999b; Hjellming & Rupen 1995).

4.3.2. *Fitting the V4641 Sgr Radio Source with a Single Finite Jet Segment*

Can a single finite jet segment fit both the radio light curves and the radio morphology? Concentrating first on the light curves, the spectral index α is -0.75 from the empirical fit. A value of $p = 0.75$ is then required to get the $t^{-1.9}$ time dependence of the optically thin decay—this value is between the $p = 0.5$ for idealized energy-conserving deceleration and the $p = 1.0$ for free expansion. The shape of the decay before and after the "kink" in the optically thin decay at 4.9 and 8.4 GHz, which occurs at MJD 51,437.23, sets the values of $t_{\mathrm{start}} = 51{,}436.78$, $t_{\mathrm{stop}} = 51{,}436.98$, and $t_0 = z_0/(\beta c) = 0.40$ days. However, the existence of the "kink" itself is due to the offset between the peaks in the radio light curve for the approaching and receding jets, an offset which appears only where relativistic time delay effects are significant. It is this time delay, which defines the kink relative to the peak, that requires $\beta \cos i = 0.4$ to fit the data, leading to the limits $0.4 \leq \beta \leq 1$ and $0 \leq i \leq 66°$.

TABLE 3

Model Parameters for the Radio Event in V4641 Sgr

Parameter	Single Jet Segment Event Model	Jet Segment Event for the Best-Fitting Two-Component Model
β	0.88	0.85
i (deg)	63	63
t_{start} (UT)	15.78	15.32
t_{stop} (UT)	15.98	15.62
$t_0 = z_0/(\beta c)$ (days)	0.40	0.40
$S_0 M_0$ (Jy)	0.138	0.0088
τ_0	200	20,000
$S_0 M_0 \tau_0$ (Jy)	27.6	176.0
Θ_0 (arcsec)	0.122	0.118
$\dot{\mu}_+$ (arcsec day^{-1})	0.457	0.43
$\dot{\mu}_-$ (arcsec day^{-1})	0.196	0.19
β_+	1.465	1.38
β_-	0.629	0.61
$\mathscr{D}_+$	0.791	0.86
$\mathscr{D}_-$	0.339	0.34
$\mathscr{Z}_+$	0.264	0.17
$\mathscr{Z}_-$	1.947	1.63

The remaining parameters for the finite jet segment model that give the best single-event fit to the radio light curves are listed in the second column of Table 3. For each required combination of β and i, the parameters $S_0 M_0$ and τ_0 are adjusted to get the best fit to the data. The remaining quantities in Table 3 are derived results from each model, including the redshifts $\mathscr{Z}_{\pm} = 1/\mathscr{D}_{\pm} - 1$. The single-event model in Table 3 for $\beta = 0.88$ is the one used for the model light curves in Figure 2. However, there is a range of models, all of which fit the constraint that $\beta \cos i = 0.4$, which are nearly as good, with the best having β between 0.84 and 0.92. For $\beta \leq 0.76$, the models have too much separation for the constraints of the 4.9 and 8.4 GHz data, whereas for $\beta \geq 0.96$, the models are too high for the early data.

The fit of the model to the data in Figure 2 is reasonable, except for two major discrepancies: the initial 1.4 GHz data points and all four 843 MHz points are considerably above the single-event model prediction, and the predicted separation of approaching and receding jets is not seen in the images on and after 17.94 UT. Instead, there is a slowly decaying optically thin remnant at the position of probable jet ejection. The September 16 images and the kink in the light curves call for the ejection of a finite jet segment; but, the optically thin remnant is more naturally produced by a more slowly decaying jet segment. In the next section, we show that this two-component model can indeed fit both the radio light curves and all of the radio images.

4.3.3. *Fitting the V4641 Sgr Radio Source with a Two-Component Jet Model*

Figure 7 shows a two-component model fit, in which the decaying central source is described by an optically thin

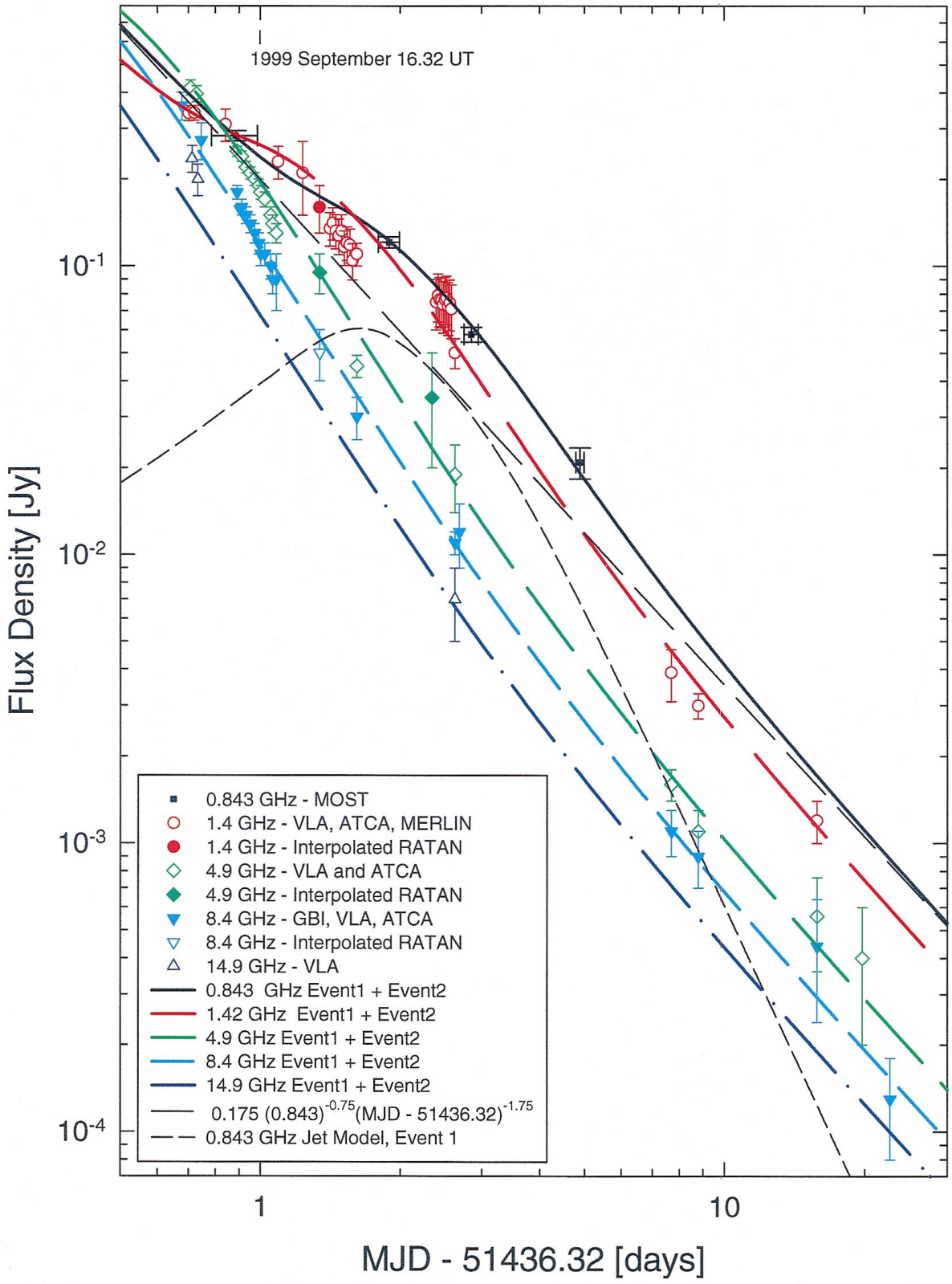

FIG. 7.—Radio flux densities in janskys plotted as a function of MJD − 51,436.32, where the symbols are the measurements from each of the seven radio telescopes and the lines are from the sum of a finite jet segment event ("Event 1") model starting at MJD − 51,436.32 and an optically thin power-law decay event ("Event 2") described by $0.175\nu_{\rm GHz}^{-0.75}({\rm MJD}-51{,}436.32)^{-1.75}$. The contributions of the two events to the 843 MHz light curve model are plotted with long- and short-dashed black lines, with their sum shown in the solid black line that fits the data reasonably well.

decay of $0.175\nu_{\rm GHz}^{-0.75}({\rm MJD}-51{,}436.58)^{-1.75}$ Jy and the jet ejection event is a modification of the model fit in Figure 2. Specifically, $M_0 S_0$ is increased to 176, the start time is moved up to MJD 51,436.32, the spectral index is steepened to −1.1, the period of jet ejection is increased to 0.3 days, and p is changed to 1, corresponding to free expansion. Free expansion is essential to making the jet segment component decay quickly enough to leave the 17.94 UT and later

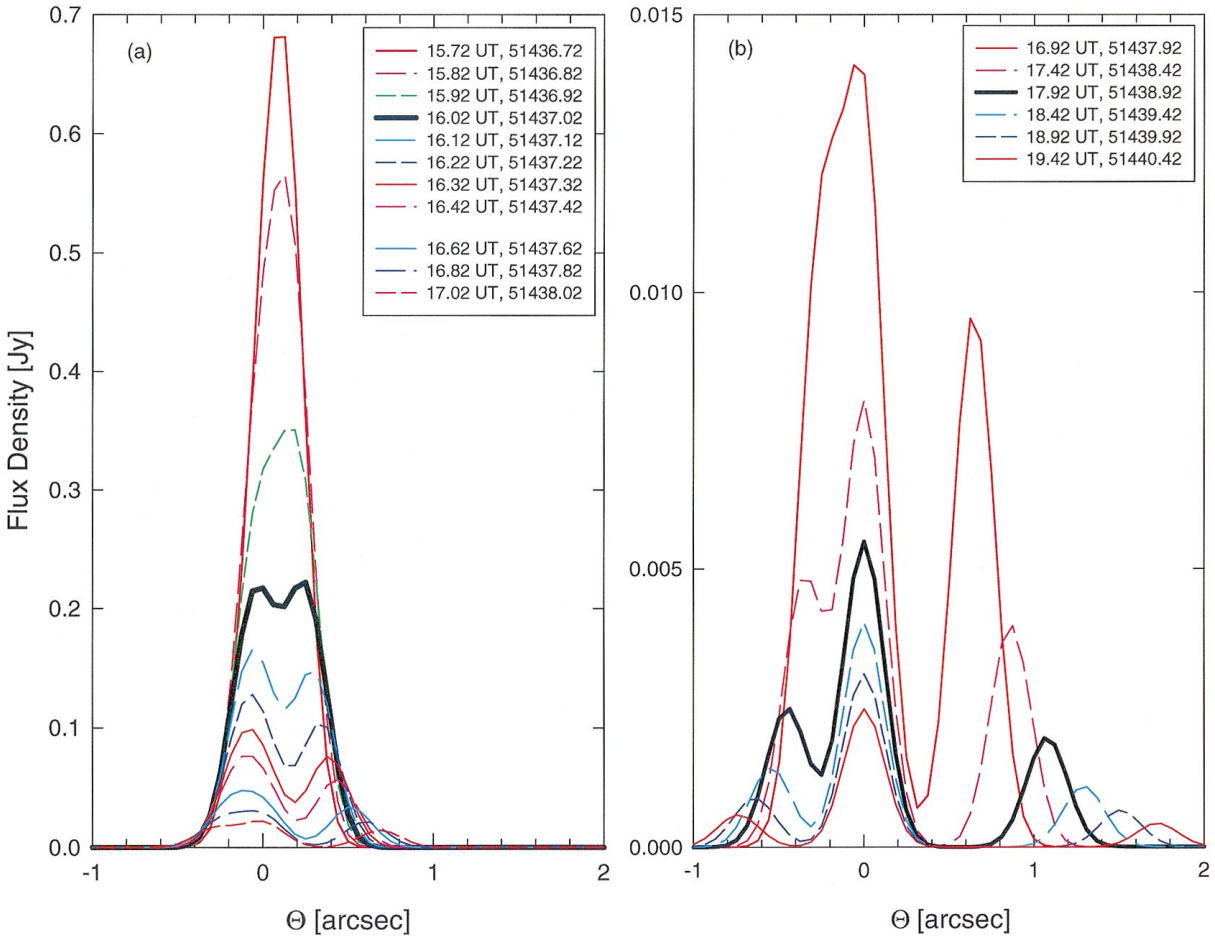

FIG. 8.—(*a*) 4.9 GHz intensity profiles for several times early in the V4641 Sgr event are plotted as a function of angular distance (Θ) from the point of ejection, with positive angles corresponding to the approaching jet at a position angle of 162° and negative angles corresponding to the opposite receding jet. (*b*) Similar intensity profiles vs. Θ for 14.9 GHz and more widely spaced time intervals later in the event. The thick black line profiles in (*a*) and (*b*) are close to the epochs imaged in Fig. 5 and roughly match the structure one sees in those images if one further smears the model emission along the position angle of the synthesized beam.

images dominated by the optically thin remnant. The separate contributions of the jet segment event and the optically thin, decaying remnant are shown in Figure 7 only for 843 MHz.

SS 433, which is the source for which the continuous conical jet model was primarily discussed by Hjellming & Johnston (1988), mostly shows steady radio emission with a constant spectral index. However, on an average of about 4 times a year SS 433 shows flares which can be fitted by the finite jet segment model discussed by R. M. Hjellming (2000, in preparation). In the context of the continuous and jet segment models, this requires only a finite period of time in which the amount of synchrotron-radiating plasma is enhanced. In this context the decaying, optically thin remnant can be produced by a jet segment of synchrotron-radiating plasma which is optically thin at all observed radio frequencies. The flux density is then given by the optically thin limit for equations (5) and (6),

$$S_{\nu,\pm,\mathrm{thin}} = \frac{S_0\, M_0\, \tau_0 (\nu/\nu_0)^{-(\gamma-1)/2}(\pi/4)}{1-(7\gamma-1)p/6} \times \left\{\left[\frac{(t-t_{\mathrm{start}})}{t_{\mathrm{scale}}}+1\right]^{1-(7\gamma-1)p/6} - 1\right\}\mathscr{D}_{\pm}^{2-\alpha}, \quad (8)$$

for $t \le t_{\mathrm{stop}}$, and

$$S_{\nu,\pm,\mathrm{thin}} = \frac{S_0\, M_0\, \tau_0 (\nu/\nu_0)^{-(\gamma-1)/2}(\pi/4)}{1-(7\gamma-1)p/6} \times \left\{\left[\frac{(t-t_{\mathrm{start}})}{t_{\mathrm{scale}}}+1\right]^{1-(7\gamma-1)p/6} - \left[\frac{(t-t_{\mathrm{stop}})}{t_{\mathrm{scale}}}+1\right]^{1-(7\gamma-1)p/6}\right\}\mathscr{D}_{\pm}^{2-\alpha}, \quad (9)$$

for $t \ge t_{\mathrm{stop}}$. There is nothing in the observed data to indicate when the optically thin jet ejection began, but some association with the ejection of the highly relativistic jet segment is reasonable. In plotting the model in Figure 7, we have therefore assumed that a linear increase from 0 to the optically thin decay formula takes place between MJD 51,436.32 and 51,436.82. The same model is also plotted in the bottom panel of Figure 1. The parameters of equations (8) and (9) cannot be determined when only an optically thin decay is observed, but an optically thin power-law decay, such as is inferred for the "second event," is predicted by these equations for $t \ge t_{\mathrm{stop}}$. The primary requirement for the difference in the two components is that for the "second component" $t_{\mathrm{scale}} = z_0/(\beta c)$ be much larger than the 0.4

days for the fast, superluminal jet because then the apparent motion per unit time will be much less. Note that this can be obtained by any combination of a larger z_0 and a smaller β.

The parameters in this two-component model are not uniquely determined, but they are consistent with all the radio data and also with the observed images. This can be seen in Figure 8, where we show the jet profiles obtained from the same model used in Figure 7, smoothed by a Gaussian with a half-power width of 0.″15. Figure 8*a* shows the 4.9 GHz prediction as a function of time for the earlier epochs, with the thick dark line representing the structure profile at 16.02 UT. Figure 8*b* illustrates the predicted 14.9 GHz emission at later epochs, with the thick dark line representing the structure profile at 17.94 UT. At 16.02 UT the sum of the flux densities of the approaching jet and the optically thin remnant is about the same as the flux density from the approaching jet, but because of the more rapid, free expansion decay of the jets, by 17.94 UT the optically thin remnant dominates the radio emission in the model. This is in reasonable agreement with the imaging results in Figure 5, particularly since the dynamic range of the image of the weak source in Figure 5*c* is only about a factor of 5. In Figure 8 one can see the progression of outward motion for the approaching (*to the right*) and receding (*to the left*) jet, and their faster decay relative to the stationary, optically thin remnant.

5. CONCLUSIONS

Only 16 hr after 1999 September 15.395 UT, when the strong rise to 12 crab flux units was detected by the *RXTE* ASM, VLA imaging shows that the radio source associated with V4641 Sgr was elongated and large, with a total extent of roughly 0.″25. Within 1.9 days this extended structure becomes too weak to be detected, leaving behind a marginally resolved, stationary remnant which slowly decayed over the following month. The rapid expansion, the strong flux density at all wavelengths, and the H I absorption spectrum all indicate a distance of $d \approx 0.5$ kpc. Both the detailed radio light curves and the VLA images at all times are well fitted by the combination of a relativistic, freely expanding jet and a residual, much more slowly decaying jet. Finite jet segment models indicate that the true twin-jet ejection velocity was $v \simeq 0.85c$, with the approaching jet being superluminal with $v_{\rm apparent} \simeq 1.4c$. The most probable value of apparent proper motion of $v \simeq 1.04c$ (see § 4.2) occurs because the observed source is a combination of the approaching jet, the receding jet, and the relatively stable, optically thin remnant. V4641 Sgr is thus the closest superluminal jet source yet seen.

The jet model gives an initial ejection date of September 15.32 UT, very close to the beginning of the strong X-ray emission, while the X-rays were already becoming harder. This may have occurred because the mildly relativistic electrons involved in the inverse Compton scattering off soft X-rays, to produce hard X-rays, were ejected from the accretion disk environment. Jet outflows perpendicular to the accretion disk have been discussed by Blandford & Payne (1982) and Blandford & Begelman (1999), and it is in these outflows that the relativistic electrons are accelerated to the higher energies needed for the observed synchrotron emission. Such jet outflows may always be associated with the accretion disk; in this picture, the transfer of the mildly relativistic electrons from a stable "corona" above the accretion disk to the jet outflows is the underlying cause of transient radio emission events. This close relationship of jet and "corona" is discussed for the case of GX 339−4 by Fender et al. (1999a). The optically thin, decaying radio emission seen in the remnant after the extended jet emission vanished probably implies that the initial highly relativistic ejection event was followed by (or accompanied) a slower outflow of relativistic electrons and magnetic fields.

The association of initial, extremely fast jets with a more slowly decaying compact remnant has been observed before in one other X-ray transient, XTE J0421+560 (=CI Cam; R. M. Hjellming et al. 2000, in preparation). This was detected in the radio in association with a comparably brief X-ray event in 1998 April (Ueda et al. 1998; Belloni et al. 1999) and also had a weak but resolved jet due to relativistic jet ejection. Unlike V4641 Sgr, CI Cam's radio remnant was almost undoubtedly due to a strong interaction of secondary ejected material with external gas, somewhat analogous to a supernova; the resulting remnant, expanding at $\sim$600–1000 km s^{-1} (A. J. Mioduszewski et al. 2000, in preparation), remained an easily detectable radio source more than a year later. In the case of V4641 Sgr, the same secondary ejection of material seemed to occur; but, without the deceleration by a surrounding dense wind, there was no additional shocking to produce further relativistic particles and consequent long-lived radio emission.

The extremely rapid evolution of the radio, optical, and X-ray events for V4641 Sgr on 1999 September 15–16 raises the question whether such brief events are often missed for other objects. The timescale of a few hours is in the range between the short interval for γ-ray bursters and the much longer interval for most of the known X-ray transients. Similarly, it is not clear whether the optical precursor to the main X-ray flare is unique to this source or a general feature which has been missed elsewhere due to poor optical coverage.

The National Radio Astronomy Observatory is a facility of the National Science Foundation operated under cooperative agreement by Associated Universities, Inc. The MOST is supported by grants from the Australian Research Council and the Science Foundation for Physics at the University of Sydney. MERLIN is operated as a National Facility by the University of Manchester, Jodrell Bank Observatory, on behalf of the Particle Physics and Astronomy Research Council (PPARC). B. M. G. acknowledges the support of NASA through Hubble Fellowship grant HF-01107.01-98A awarded by the Space Telescope Institute, which is operated by the Association of Universities for Research in Astronomy, Inc., for NASA under contract NAS–26555. We are grateful to the observers, programmers, and VLA operations staff who were generous in letting us have the small portions of time that allowed the VLA coverage reported in this paper. We also thank Ketan Desai for providing the model-fitting program OMFIT in AIPS, used for fitting Gaussian models to the September 16 visibilities. Finally, the rapid exchange of preliminary results among many X-ray, optical, and radio observers was essential in allowing so much to be determined about this remarkable but brief event; we are very happy to be able to thank the many people who made this possible.

REFERENCES

Blandford, R. D., & Begelman, M. 1999, MNRAS, 303, L1
Blandford, R. D., & Payne, D. G. 1982, MNRAS, 199, 883
Belloni, T., et al. 1999, ApJ, 527, 345
Briggs, D. A. 1995, Ph.D. thesis, New Mexico Tech
Djorgovski, S. G., Gal, R. R., Mahabel, A., Galama, T., Bloom, J., Rutledge, R., Kulkarni, S., & Harrison, F. 1999, Astron. Telegram 44
Esin, A. A., Lasota, J.-P., & Hynes, R. I. 2000, A&A, 354, 987
Fender, R. P., et al. 1999a, ApJ, 519, L165
Fender, R. P., Garrington, S. T., McKay, D. J., Muxlow, T. W. B., Pooley, G. G., Spencer, R. E., Stirling, A. M., & Waltman, E. B. 1999b, MNRAS, 304, 865
Fich, M., Blitz, L., & Stark, A. A. 1989, ApJ, 342, 272
Fishman, G., et al. 1989, in Proc. Gamma-Ray Obs. Sci. Workshop 2, ed. N. Johnson (NASA CP-3137), 39
Fukugita, M., Shimasaku, K., & Ichikawa, T. 1995, PASP, 107, 945
Gaensler, B. M., Campbell-Wilson, D., Hunstead, R. W., & Sault, R. J. 1999, IAU Circ. 7256
Goranskij, V. P. 1978, Astron. Tsirk., 1024, 3
———. 1990, Inf. Bull. Variable Stars 3464
Green, D. W. E. 1999, IAU Circ. 7277
Harmon, B. A., et al. 1992, in Proc. Compton Obs. Sci. Workshop, ed. C. R. Shrader, N. Gehrels, & B. Dennis (Washington, DC: NASA), 69
Harmon, B. A., et al. 1995, Nature, 374, 703
Hjellming, R. M. 1996, in ASP Conf. Ser. 212, Accretion Phenomena and Related Outflows, ed. D. T. Wickramasinghe, G. V. Bicknell, & L. Ferrario (San Francisco: ASP), 53
Hjellming, R. M., & Johnston, K. J. 1988, ApJ, 328, 600
Hjellming, R. M., & Rupen, M. P. 1995, Nature, 375, 464
Hjellming, R. M., Rupen, M. P., & Mioduszewski, A. J. 1999, IAU Circ. 7254
in 't Zand, J., Heise, J., Bazzano, A., Cocchi, M., Di Ciolo, L., & Muller, J. M. 1999, IAU Circ. 7119
Jain, R., & Bailyn, C. 2000, IAU Circ. 7400
Kato, T., Uemura, M., Stubbings, R., Watanabe, T., & Monard, B. 1999, Inf. Bull. Variable Stars 4777
Kellermann, K. I. 1966, ApJ, 146, 621
Kulkarni, S. R., & Heiles, C. 1988, in Galactic and Extragalactic Radio Astronomy, ed. G. L. Verschuur, K. I. Kellermann, & E. Bouton (2d ed.; Berlin: Springer), 98
Kuulkers, E., et al. 1999, MNRAS, 306, 919
Markwardt, C. B., Swank, J. H., & Marshall, F. E. 1999, IAU Circ. 7120
McCollough, M. L., Finger, M. H., & Woods, P. M. 1999, IAU Circ. 7257
Mirabel, I. F., & Rodríguez, L. F. 1994, Nature, 371, 46
Orosz, J. A., Remillard, R. A., Bailyn, C. D., & McClintock, J. E. 1997, ApJ, 478, L83
Shklovskij, I. 1960, Astron. Zhurnal, 37, 345
Smith, D. A., Levine, A. M., & Morgan, E. H. 1999, IAU Circ. 7253
Stubbings, R. 1999, IAU Circ. 7253
Van der Laan, H. 1966, Nature, 211, 1131
Ueda, Y. 1998, ApJ, 508, L167
Wijnands, R., & van der Klis, M. 2000, ApJ, 528, L93
Williams, G. V. 1999, IAU Circ. 7277